Numerical exploration of starting process in supersonic nozzle

S. Saha and D. Chakraborty
Computational Combustion Dynamics Division
Defence Research and Development Laboratory
Hyderabad, India

ABSTRACT

The starting process in a supersonic nozzle is numerically simulated. The Navier Stokes equations, in axisymmetric form, are solved using a higher order spatial and temporal accurate scheme. Good comparisons between experimental and numerical values of various flow parameters form the basis of further analysis. The insight of the starting process in the nozzle, namely, the movement of primary and secondary shocks and contact discontinuity, has been obtained through analysis of various flow parameters. It has been observed that the inviscid phenomenon is more predominant in the flow development process. Parametric studies have been carried out to determine the effect of nozzle divergence angle on the starting process.

NOMENCLATURE

a_0	speed of sound ahead of incident shock
C_s	speed of incident shock
E	total energy, defined as $E = e + 0{\cdot}5\ (u^2 + v^2)$
e	internal energy, defined by ideal gas equation $p = (\gamma - 1)\rho e$
h_c	height of nozzle throat
M_2	Mach number of flow behind the incident shock wrt. incident shock
P	pressure
q_x, q_y	heat flux in x and y direction.
R	gas constant
S_1	constant in Sutherland's law for viscosity variation
T	temperature
T_0	reference temperature in Sutherland's law for viscosity variation
t^*	non dimensional time
x	co-ordinate direction along axis
y	coordinate direction along radius
γ	specific heat ratio
λ, μ	bulk and molecular Viscosity
μ_0	viscosity at reference temperature T_0
$\tau_{xx}, \tau_{xy}, \tau_{yy}, \sigma_H$	viscous stress terms

1.0 INTRODUCTION

Short duration facilities like shock tunnel and expansion tubes are very important to study hypersonic flows. They can generate the required combination of temperature and pressure for simulating the high Mach number flight conditions. These facilities are used extensively all over the world to characterise the hypersonic flows[1-4]. Good test data can also be obtained for flight propulsion performance prediction for hydrogen fueled scramjet[5-6], although this short duration (~ 5ms) may not be adequate to study the hydrocarbon fueled scramjet propulsion system.

Paper No. 3087. Manuscript received 23 April 2006, revised 28 June 2006, accepted 10 October 2006.

A basic schematic of a shock tunnel is shown in Fig. 1. The shock tunnel consists of a driver tube filled with a high pressure gas, a driven tube filled with test gas at low pressure, a supersonic nozzle evacuated to low pressure, and finally a test section. When the pressure in the driver tube is high enough, the primary diaphragm breaks and sends a planar shock wave down the driver tube. This incident shock splits into two waves by reflecting at the end of the driven tube; one is a reflected shock wave goes back upstream, and other is a primary shock wave that breaks the secondary diaphragm sending flow through the nozzle. The gas in the driven tube behind the reflected shock wave forms the reservoir of high pressure and high temperature gas for the nozzle flow. A mean flow can be established after the primary shock and the secondary shock pass the nozzle outlet and test can be performed until the nozzle flow becomes contaminated with the driver gas. The schematic of flow behavior occurring inside the shock tube after the diaphragm is ruptured is presented in Fig. 2 and the upstream movement of reflected normal shock wave is shown in Fig. 3. Further details of shock tunnel operation are available in Ref. 7.

The prediction of the starting process of the shock tunnel is very important to determine the run time of the facility. This phenomenon is induced by unsteady shock/boundary layer interaction. Moreover, there exist factors like reflected waves in the nozzle that affect the starting up process. Consequently, the actual flow field of the shock tunnel is more complicated than obtained from a one-dimensional theory or method of characteristics. The knowledge of the starting process in a supersonic nozzle is also important to predict the side loads caused during the start-up and shut down transients of a rocket nozzle. In a few milliseconds, multiple shock waves and contact discontinuities with increasing interaction occur and act on the internal nozzle walls. Consequently, the pressure distribution may deviate from its usual symmetrical shape, producing significant side loads that would be detrimental to the mechanical structure of the nozzle. The mechanism of shock wave propagation during the nozzle start up process is quite complex and a fundamental knowledge of flow physics is still needed to understand the starting process.

Experimental investigations of transient nozzle flow field driven by a shock tube were carried out by Smith[8], Amann[9-10] and Saito *et al*[11]. Amann[9] studied the influence of several parameters such as nozzle half angle, throat and the nozzle inlet radius etc., on the starting process. Special interest was paid to the duration of the starting process as it reduces the useful testing time of short duration facility. Chopra *et al*[12] carried out an experimental investigation of a transient shock wave interaction in the rocket nozzle in a shock tube and found the existence of transient radial wave superimposed on base reflected axial shock wave.

Most of transient numerical simulations of shock tunnel with nozzle were in two dimensional or axisymmetric planes due to the large requirement of computer time for three-dimensional calculation. Prodromou and Hiller[13], Igra *et al*[14] have performed numerical simulation of transient shock tunnel flow field using two dimensional Euler equations and obtained good agreement with the experimental data of Amann[9] and Saito *et al*[15]. Tokarcik-Polsky and Cambier[16], Chopra *et al*[12] studied the transient flow field using two dimensional Navier Stokes equations. These studies gave detailed information on flow characteristics in the nozzle of shock tunnel. Mournoval and Hadjadi[17-18] have studied the transient flow field of a supersonic nozzle driven by shock tube using a fifth order WENO scheme and obtained good agreement with experimental results. Results of both axisymmetric and two dimensional Euler equations are compared. Although, the nature of the flow remains similar, more complex phenomena were present for axisymmetric configuration than for the plane one. This is partly due to the appearance of an internal shock, resulting from the focalisation of the characteristics lines induced by the expansion fan, and to its interaction with the secondary shock. Their simulation indicates that Mach wave reflected in the divergent part of the nozzle plays an important role in generating side loads. Kancko and Nakamura[19] studied the transient flow field of the Nagoya University shock tunnel at M = 8 using an axisymmetric compressible finite volume N-S Solver with the MUSCL and Roe's FDS in space and 4th order Runge-Kutta Scheme in time. The numerical results well represented the time variation of the complicated flow structure in the nozzle.

Chen *et al*[20] examined the flow structure of start up and shut down processes of the J-2S rocket engine (precursor of US space shuttle main engine). Nasuli and Onofri[21] and Wang[22] studied the transient flow field of Vulcain and SSME nozzle respectively. Their studies showed that the transient flow field is characterised by two main vortical regimes; the first created by the viscous separation at the wall, the second by an inviscid production of vorticity behind the recompression shock that take place in the divergent section and these vortical structures cause wall pressure fluctuations. It is clear that detailed investigation of starting process of nozzle flow is necessary for better understanding of hypersonic flow characteristics in a shock tunnel.

In the present work, the transient flow field in a nozzle and driven by a shock tube is explored numerically using a commercial CFD solver Fluent[23]. Both inviscid and viscous models are used to extract the effect of viscous and pressure forces on the flow establishment process. The experimental condition of nozzle starting process[9] is taken as the validation case and the flow parameters are compared with the experimental and other numerical simulation results. Parametric investigations are also conducted to study the effect of the nozzle divergence angle in the flow starting process.

2.0 EXPERIMENTAL CONDITION FOR VALIDATION

The experimental condition of transient nozzle flow of Amann and Reichenbach[9] and Amann[10] has been selected as the validation case in the present study. The schematic of the nozzle is shown in Fig. 4. The experimental arrangement used side plates in the supply tube to reduce viscous effects upstream of the nozzle. The test was initiated with a Mach 3 shock in air upstream of the nozzle with a 15° semi-divergence angle. The shock propagated into stagnant gas with T = 293K and P = 6·3KPa. The nozzle had a rounded inlet with radius of r = 10mm and a throat half width of h = 3mm.

3.0 ANALYSIS

3.1 Governing equation

The axisymetric time dependent equations for viscous flow in a Cartesian coordinates are given in a conservation vector form as

$$\frac{\partial \mathbf{U}}{\partial t}+\frac{\partial \mathbf{F}}{\partial x}+\frac{1}{y}\frac{\partial}{\partial y}(y\mathbf{G})=\frac{\mathbf{H}}{y}$$

$$U=\begin{bmatrix}\rho\\ \rho u\\ \rho v\\ \rho E\end{bmatrix}\quad F=\begin{bmatrix}\rho u\\ \rho u^2+p+\tau_{xx}\\ \rho uv+\tau_{xy}\\ (\rho E+p)u+u\tau_{xx}+v\tau_{xy}-q_x\end{bmatrix}$$

$$G=\begin{bmatrix}\rho v\\ \rho uv+\tau_{xy}\\ \rho v^2+p+\tau_{yy}\\ (\rho E+p)v+u\tau_{xy}+v\tau_{yy}-q_y\end{bmatrix}\quad H=\begin{bmatrix}0\\ 0\\ -p+\sigma_H\\ 0\end{bmatrix}$$

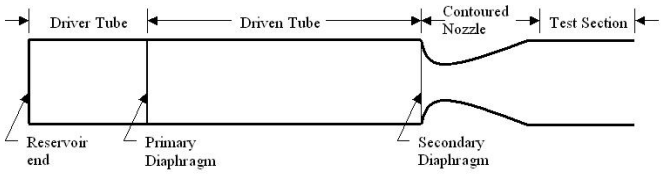

Figure 1. Schematic of a shock tunnel.

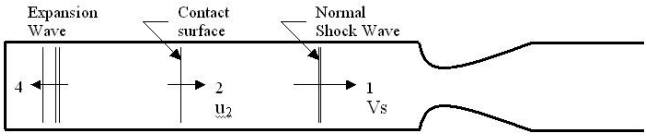

Figure 2. Flow behavior occurring inside the shock tube after diaphragm is ruptured.

Where ρ, p, u, v are the density, pressure and flow velocity components in x and y direction respectively. The total energy is defined as $E = e + ½(u^2 + v^2)$

The viscous stress terms are expressed as

$$\tau_{xx} = (\lambda + 2\mu)\frac{\partial u}{\partial x} + \lambda \frac{1}{y}\frac{\partial}{\partial y}(yv)$$

$$\tau_{yy} = (\lambda + 2\mu)\frac{\partial v}{\partial y} + \lambda\left(\frac{\partial u}{\partial x} + \frac{v}{y}\right)$$

$$\tau_{xy} = \mu\left(\frac{\partial u}{\partial y} + \frac{\partial v}{\partial x}\right)$$

$$\sigma_H = (\lambda + 2\mu)\frac{v}{y} + \lambda\left(\frac{\partial u}{\partial x} + \frac{\partial v}{\partial y}\right)$$

The two coefficients λ and μ are related by Stokes Law 3λ+2μ = 0 and q_x and q_y are the heat flux rate in the x, y direction. The systems of equations are closed with the ideal gas equation of state $p = (\gamma - 1)\rho e$.

In the present calculation it is assumed that the coefficient of viscosity is dependent only on the temperature and followed Sutherland Viscosity Law

$$\frac{\mu}{\mu_0} = \left(\frac{T}{T_0}\right)^{\frac{3}{2}} \frac{T_0 + S_1}{T + S_1}$$

Where S_1 is a constant value of 110K and μ_0 is the coefficient of viscosity at a reference state. The constant value of 0·72 for the Prandtl number is also assumed.

3.2 The computational grid

To capture the flow transient it is necessary to adopt a very fine grid in the computational domain. An axisymmetric model representing the experimental condition of Amann[10] was generated and meshed with quadrilateral cell through Gambit – the grid generator module for Fluent software[23]. In axisymmetric solver, one applies curvilinear grids in the axial and radial directions and no grid is used in the azimuthal direction. Owing to this simplification, axisymmetric conditions are prescribed along the central line of the nozzle. The

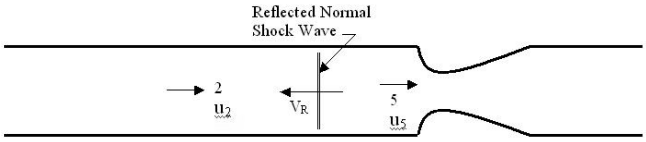

Figure 3. Reflected normal shock wave moving upstream.

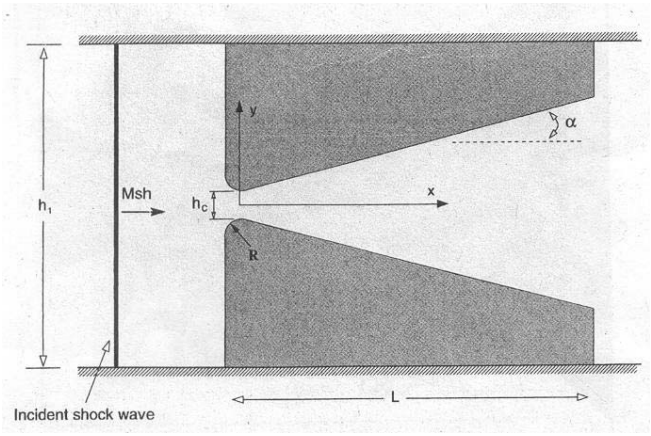

Figure 4. Schematic of the nozzle with shock tube.

grid distribution in the nozzle is shown in Fig. 5. Approximately 0·4 million nodes are used in the computational domain. Every third line of the grid in the x direction is shown in the figure to indicate the nature of the grid. The closer view of the nozzle near the throat is also shown in the figure. The minimum spacing of the grid is 0·1mm near the throat, while the maximum is about 0·65mm near the exit. The grid is shown to be adequate to capture all the essential features of flow fields as demonstrated from the grid independence study presented later.

3.3 Initial and boundary conditions

The initial condition corresponds to the moment when a plane incident shock with Mach 3 passes a stationary medium at P = 6·3KPa and P = 293K and reaches to the shock tube end wall, where the nozzle entrance is located. The test gas is air with γ = 1 4. The inlet boundary conditions are calculated assuming stationary shock and the normal shock relations are used. Across a normal shock corresponding to M = 3, the static pressure, temperature and velocity of the flow are 65·1KPa, 785K and 227ms^{-1} respectively. And with speed of shock $C_S = M * \sqrt{\gamma RT} = 1029\,\text{ms}^{-1}$, the flow behind the normal shock travel at $M_s = \frac{C_S - M_2}{\sqrt{\gamma RT_2}} = 3 \cdot 5$ The total temperature and the total pressure of the flow are 195KPa and 1,074K. The following flow conditions are summarised in Table 1 are used in the simulation:

Table 1
Initial and Boundary Conditions

Condition	Static pressure (KPa)	Static temperature (K)
Initial condition	6·3	293
Inlet boundary	65·1	785
Outlet boundary	6·3	293

The no slip boundary conditions are used on solid wall and the wall temperature is kept as 293K.

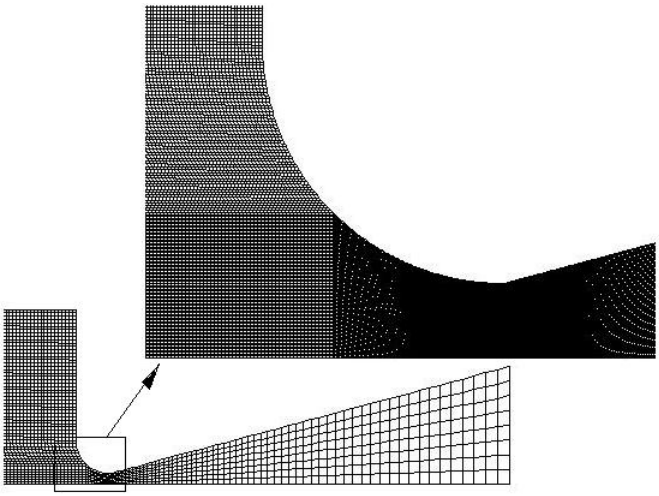

Figure 5. Grid distributions in the nozzle
(blown up view near the throat is also shown).

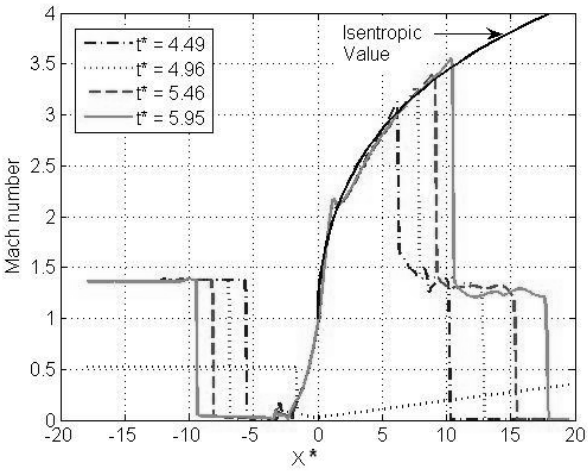

Figure 8. Centreline Mach number
distributions at various instants of time.

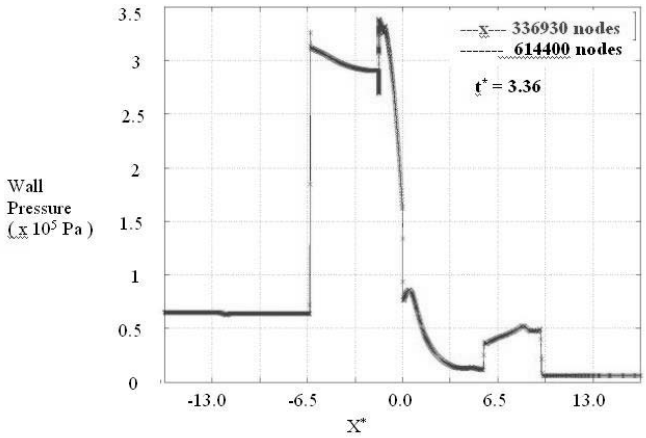

Figure 6. Comparison of axial distribution
of surface pressure in two different grids.

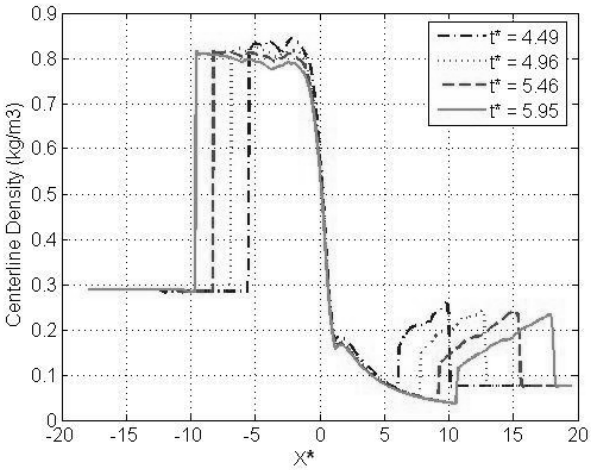

Figure 9. Centreline density distributions at various instants of time.

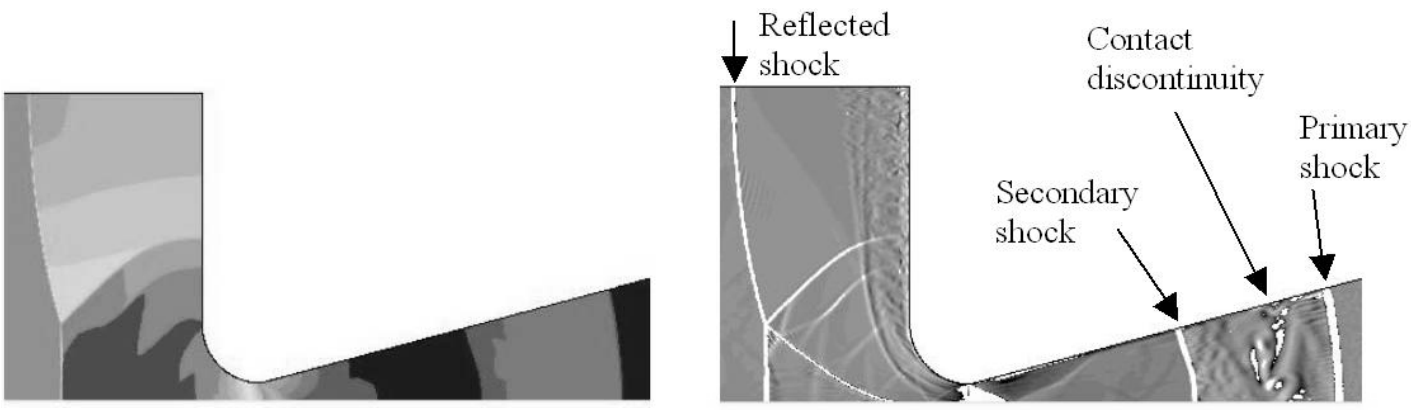

(b) (a)

Figure 7. Density plot at t^* = 3·97 (a) Contour plot, (b) Numerical Schlieren image.

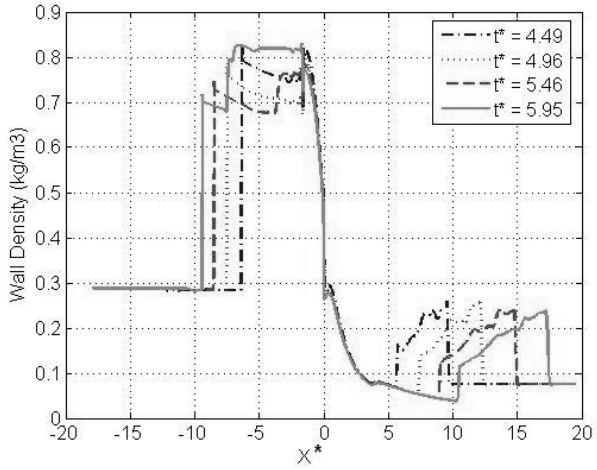

Figure 10. Density distributions near wall at various instants of time.

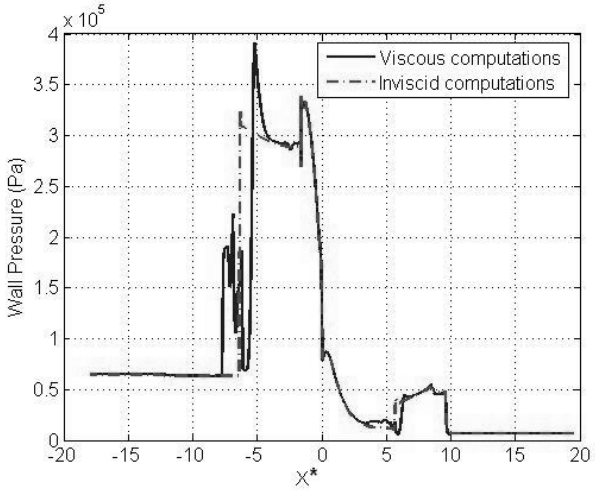

Figure 11. Wall pressure distribution for inviscid and viscid simulation at t^* = 3·40.

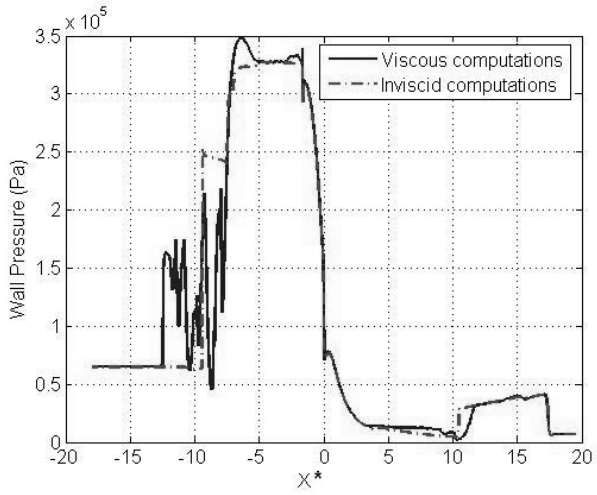

Figure 12. Wall pressure distribution for inviscid and viscid simulation at t^* = 6·57.

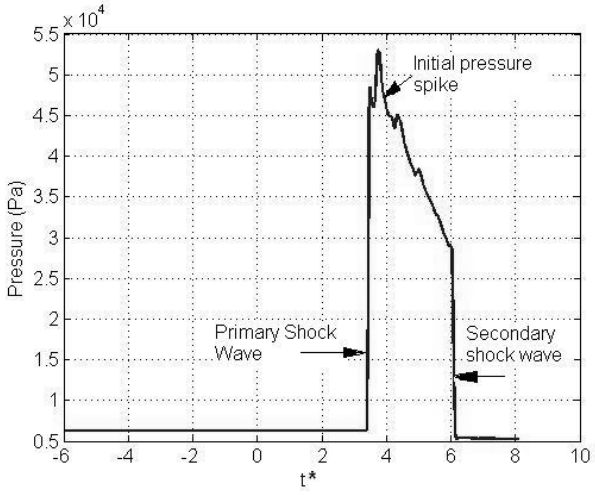

Figure 13. Wall pressure trace at x^* = 8·05 plane.

4.0 RESULTS AND DISCUSSIONS

The transient flow simulations start after the diaphragm is ruptured and incident normal shock wave travels downstream towards the nozzle. A second order explicit upwind scheme is employed to solve the governing equations of mass, momentum and energy. A fixed CFL number of 0·2 is chosen for the transient calculations. The computed axial distribution of wall pressure at t^* = 3·36 is compared with two different grids namely 0·614 and 3·37 million in Fig. 6. The time is normalised as $t^* = t\ a_0/h_c$, a_0 is the speed of sound of gas initially at rest and h_c is the throat diameter. The location of nozzle throat is chosen as origin. We can see that the results remain the same with two different grids, thus demonstrating the grid independence of the results. It can also be seen that the flow expands until it reaches the secondary shock. Subsequently, the pressure increases gradually between secondary shock and the primary shock. The instantaneous pressure contour and the numerical schlieren in the flow field at t^* = 3·97 is shown in Fig. 7 to depict clearly the primary shock, secondary shock, contact discontinuity and the reflected normal shock. On the arrival of the incident shock wave, its upper and lower parts are reflected from the shock tube end wall; while the portion at the nozzle throat is transmitted unchanged. As a result, shock waves are created at the upper and lower edges of the nozzle throat and propagate towards the plane of symmetry. Two shock waves soon collide at the plane of symmetry and secondary shock waves are created behind the primary shock due to repeated reflection between the nozzle walls. The primary shock can be clearly seen propagating into the medium at rest, while secondary shock is moving relative to the gas. The contact discontinuity is clearly seen in the schlieren picture; It is getting distorted owing to a Ritchmyer – Meshkov instability described in Ref. 1.

The computed centerline Mach number distribution at different instants of time(t^* = 4·49 4·96 5·46 and 5·95) is presented in Fig. 8 along with the isentropic values. The movement of primary shock, secondary shock and the reflected shock is clearly visible. The axial variations of central line and wall density distribution at different instants of time are presented in Figs 9 and 10 respectively. The axial distribution of nozzle wall pressure for the viscous calculation has been compared with the inviscid results in Figs 11 and 12 at two time instants t^* = 3·40 and 6·57. Although there are some differences near the nozzle throat the flow field in the downstream region does not alter significantly between the viscous and the inviscid simulations. Nasuli and Onofri[21] have also observed that the inviscid phenomena are predominant in the flow process under transient condition. The speeds of the primary and secondary shock are

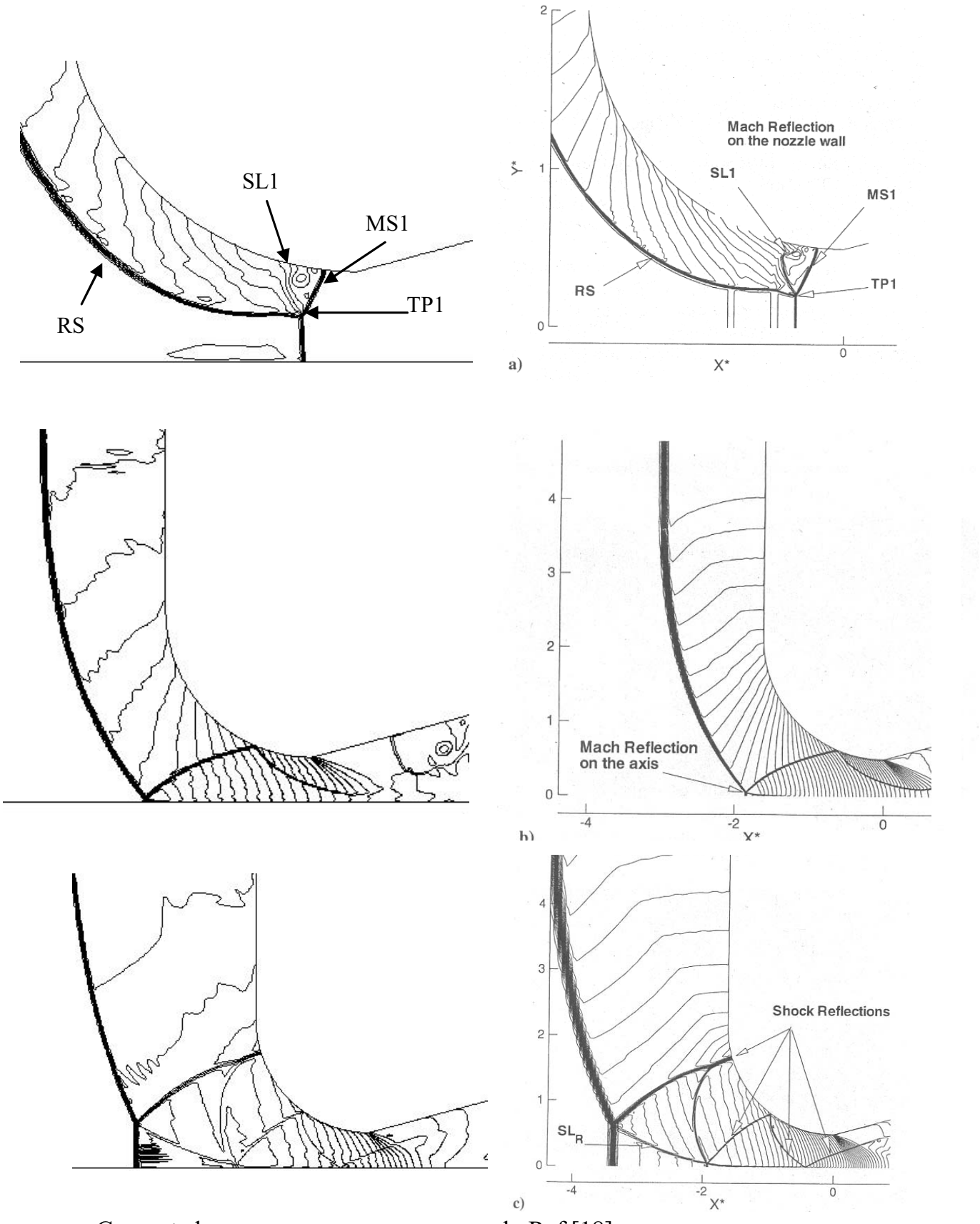

a. Computed b. Ref [18]

Figure 14. Comparison of computed density contours with Mouronval and Hadjadi[18] at t^* = –8·32e–2, 0·59, and 1·70.

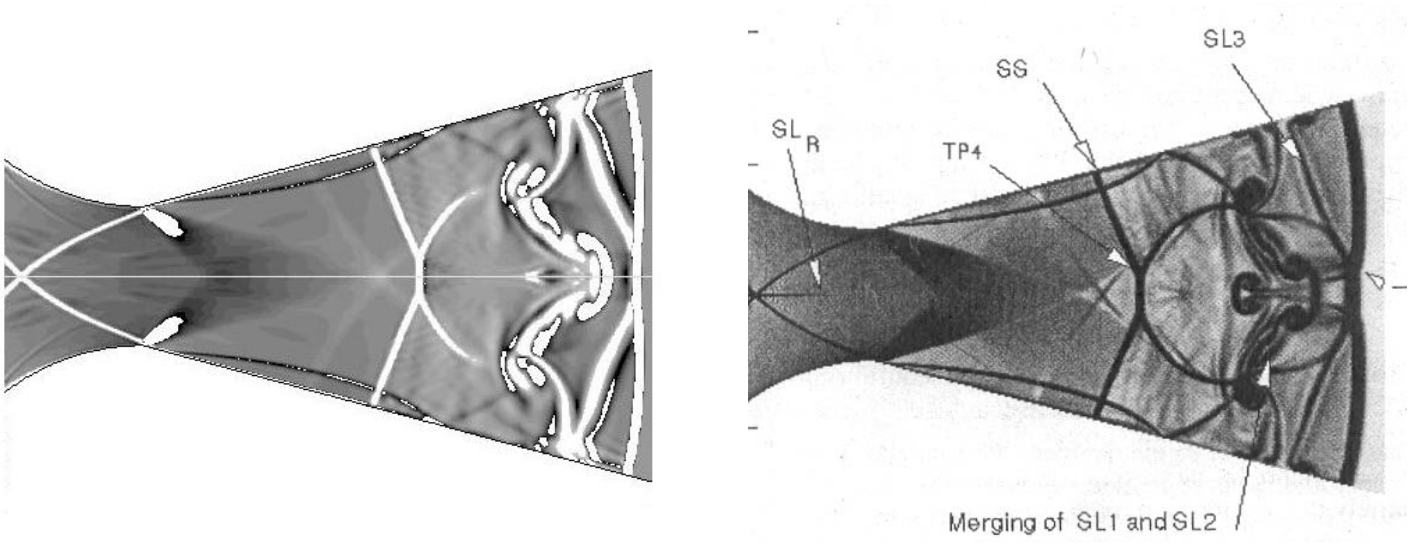

Figure 15. Numerical Schlieren images (a) computed, (b) Ref. 18.

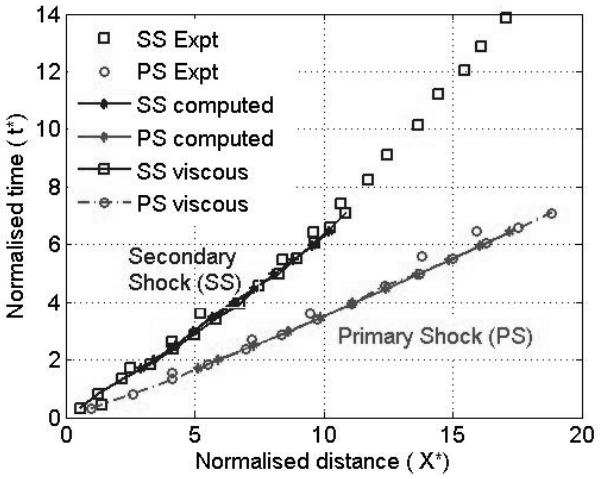

Figure 16. Comparison of computed primary and secondary shock trajectory with experimental results[9].

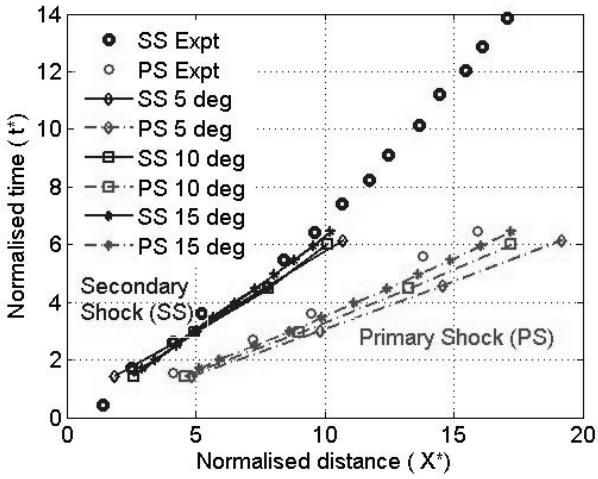

Figure 17. Computed primary and secondary shock trajectory with different nozzle divergence angle.

calculated from its position at different instant of time. It has been found from the calculation that primary shock reach the nozzle exit at $t^* = 7{\cdot}0$. The wall pressure trace (wall pressure *Vs* time) at x^* ($= x/hc$) of 8·05 is presented in Fig. 13 to depict the flow evolution and it can be seen that the steady state flow get established after the passage of the secondary shock.

The computed density contour in the upstream of the nozzle throat ($x^* < 0$) at time ($t^* = -8{\cdot}32\ e-2$, 0·59 and 1·70) has been presented in Fig. 14 to describe the early stages of the starting process in more detail. These results are compared with the numerical simulation of Mournval and Hadzadi[18] who have used a fifth order WENO scheme[24] and third order explicit Runge-Kutta method for time marching. Good qualitative comparisons have been obtained. As soon as the incident shock reaches the nozzle entrance its outer part reflects on the wall, whereas the inner part enters the nozzle. The simulation captures the early stages of starting process including the Mach reflection on the wall and the subsequent phenomena of Mach reflection at nozzle axis and further shock reflections. The emergence of the slip line due to meeting of reflected shock (RS), transmitted shock (PS) and the Mach stem (MS1) at triple point TP1 is clearly captured in Fig. 14(a) in the simulation and compare well with the results of Ref. 18. The numerical schlieren of the flow field near the nozzle throat at early stages of the start up process at $t^* = 1{\cdot}14$ is compared with that of Mouronval and Hadjadi[18] in Fig. 15. The complex flow structure between the primary shock and contact discontinuity is captured in the simulation.

The comparisons of experimental and the numerical values of the primary and the secondary shocks trajectories are presented in Fig. 16. The axial distance is normalised by the nozzle throat diameter and the time is normalised by t^* as defined earlier. The position of primary and the secondary shocks at any instance of time has been determined from the location at which the wall pressure is discontinuous. The excellent agreement between the experimental and numerical values demonstrates that the simulation has captured all the features of the flow accurately. The shock speed computed from the viscous calculation is also presented in the figure to demonstrate that viscosity does not have a significant role in altering the flow features.

To study the influence of nozzle divergence angle on the flow starting process, several computations were carried out for a range of nozzle half angles $\alpha = 5°$, 10° and 15° while keeping all other parameters same. The computed primary and the secondary shock speeds with different divergence angles are presented in Fig. 17. The results indicate that the starting process is delayed if the nozzle divergence angle is increased. This confirms the previous study reported by Amann[10].

5.0 CONCLUSIONS

Numerical simulations are carried out to study the transient flows in a supersonic nozzle driven by a shock tube using second order accurate spatial and temporal schemes. The simulation captures all the essential features of the flow field including the movement of primary and secondary shocks, contact discontinuity etc. A very good comparison is obtained between the experimental and numerical values of primary and secondary shock speeds. Fine details of the flow structures at various stages of development have been captured accurately as is evident from the excellent agreement between the experimental and numerical flow parameters. Although, the inviscid and viscous pressure traces differ near the nozzle throat, the flow field in the downstream region remains the same. This indicates that inviscid phenomena are predominant in finding out the effect of vortical structure in the nozzle flow transient process. Parametric studies with different nozzle angles reveals that the transient process is delayed if the nozzle divergence angle is increased.

REFERENCE

1. JACOB, P.A. Simulation of transient flow in a shock tunnel and a high mach number nozzle, NASA- CR – 187606, 1991.
2. STALKER, R.J. A study of free-piston shock tunnel, *AIAA J*, 1967, **5**, (12), pp 2160-2165.
3. HORNUNG, H.G. Performance data of new free-piston shock tunnel at GALCIT, AIAA, 1992, Paper No 92-3943.
4. ITOH, K., UEDA, S., TANNO, H., KOMURO, T. and SATO, K. Hypersonic Aerothermodynamics and scramjet research using high enthalpy shock tunnel, *Shock Waves*, 2002, **12**, pp 93-98.
5. PAULL, A., STALKER, R.J. and MEE, D.J. Experiments on supersonic combustion ramjet propulsion in a shock tunnel, *J Fluid Mechanics*, August 1995, **296**, pp 159-183.
6. JIALING, L. and WEIXIONG, L. Recent progress of CARDC in experimental and computational scramjet research, Proceeding of East West High Speed Flow Field Conference (EWHSFF 2005), Beijing, China, pp 24-30.
7. GAYDON, A.G. and HURLE, I.R. *The Shock Tube in High Temperature Chemical Physics*, Reinhold, New York, USA, 1963.
8. SMITH C.E. The starting process in a hypersonic nozzle, *J Fluid Mechanics*, 1966, **24**, pp 625-640.
9. AMANN H.O. and REICHENBACH, H. *Unsteady Flow Phenomena in Shock Tube Nozzle, Recent Development in Shock Tube Research*, edited by BUSHADER, D. and GRIFFITH, W. Stanford University Press, Stanford, CA, USA, 1973, pp 96-112.
10. AMANN, H.O. Experimental study of the starting process in a reflection nozzle, *Physics of Fluids*, 1969, **12**, (5), pp 150-153.
11. SAITO, T., TIMOFEEV, E.V., SUN, M. and TAKAYAMA, K. Numerical and experimental study of 2D nozzle starting process, Proceedings of the 22nd International Symposium of Shock Waves, 1999, London, UK, Paper No 4090.
12. CHOPRA, H.S., GREATRIX, D.R. and KAWALL, J.G. Transient shock wave interaction with rocket nozzle – cold flow study, 2003, AIAA Paper 2003 – 4669.
13. PRODROUMOU, P. AND HILLIER, R. Computation of Unsteady Nozzle Flows, Proceedings of the 18th International Symposium on Shock Waves, 1991, pp 1113 – 1117.
14. IGRA, O., WANG, L., FALCOVITZ, J. and AMANN, O. Simulation of starting flow in a wedge like nozzle, *Shock Waves*, 1998, **8**, pp 235-242.
15. SAITO, T. and TAKAYAMA, K. Numerical simulation of nozzle starting process, *Shock Waves*, 1999, **9**, pp 73-79.
16. TOKARICK–POLSKY, S. and CAMBIER, J.L. Numerical study of transient flow phenomena in shock tunnel, *AIAA J*, 1994, **32**, (5), pp 971-978.
17. MOURONVAL, A.S., HADJADI A.A., KUDRYAVTSEV, A. and VANDROMME, D. Numerical investigation of transient nozzle flows, *International J Shock Waves*, 2002, **12**, (5), pp 403-411.
18. MOURONVAL, A.S. and HADJADI A. Numerical study of the starting process in a supersonic nozzle, *J Propulsion and Power*, **21**, (2), 2005, pp 374-378.
19. KANEKO, M. and NAKAMURA, Y. Numerical investigation of unsteady flow field with shock interaction in a shock tunnel, AIAA paper 2001-0742, 2001.
20. CHEN, C.L., CHAKRAVARTHY, S.R. and HUNG, C.M. Numerical investigation of separated nozzle flows, *AIAA J*, **32**, (9), 1994, pp 1836-1843.
21. NASULI, F. and ONOFRI M. Viscous and inviscid vortex generation during startup of rocket nozzle, *AIAA J*, May 1998, **36**, (5), pp 809-815.
22. WANG, T. Transient Two-Dimensional Analysis of side load in liquid rocket engine nozzle, AIAA Paper 2004 – 3680, 2004.
23. Fluent Version 6.0 User' guide, Fluent Incorporated, New Hampshire, 2001
24. JIANG G. and SHU C.W. Efficient implementation of weighted essentially non-oscillatory scheme, *J Computational Physics*, **126**, (1), 1996, pp 202 – 228.